Graphene-ZnO Hollow Microspheres Composite for Supercapacitor Applications

Abqari Luthfi Albert Abdullah[1, a], Shahidan Radiman[2, b], Wee Siong Chiu[3, c], Muhammad Azmi Abdul Hamid[2, d] and Fadhlul Wafi Badrudin[1, e*]

[1]Physics Department, Centre for Defence Foundation Studies, National Defence University of Malaysia, Sungai Besi Camp, 57000 Kuala Lumpur, Malaysia

[2]School of Applied Physics, Faculty of Science and Technology, Universiti Kebangsaan Malaysia, 43600 Bangi, Selangor, Malaysia

[3]Low Dimensional Materials Research Center, Department of Physics, Faculty of Science, University of Malaya, 50603 Kuala Lumpur, Malaysia

[a]albert@upnm.edu.my, [b]shahidan@ukm.edu.my, [c]w.s.chiu@um.edu.my, [d]azmi@ukm.edu.my, [e]fadhlul@upnm.edu.my

*Corresponding author: Tel: +60 13 4668097

Keywords: Graphene, zinc oxide, hollow sphere, composites, solvothermal

Abstract. Through a facile solvothermal synthesis process, a graphene-ZnO microspheres composite was produced at 180 °C for 24 hours. Raman spectroscopy, X-ray diffraction (XRD), field emission scanning electron microscopy (FESEM) and transmission electron microscopy (TEM) were used to analyse the morphological structures of the materials. The analysis revealed that homogeneous microspheres assembled by hexagonal phase wurtzite ZnO nanoparticles were decorated on the graphene sheets via graphene oxide (GO) functional groups. The ZnO nanoparticles are about 30 nm in size and the microspheres are hollow. A possible growth mechanism for the formation of ZnO hollow microspheres anchored on graphene sheets has been proposed. Cyclic voltammetry (CV), galvanostatic charge-discharge (GCD) and electrochemical impedance (EIS) were used to evaluate the electrochemical performance of the composite. At a scan rate of 1 mV/s, the graphene-ZnO hollow microspheres (rGS-ZnO(HMs)) composite electrode demonstrated enhanced specific capacitance of 40.70 F/g with respective energy and power densities of 5.75 W h/kg and 1.97 kW/kg.

Introduction

Graphene, a two-dimensional atom-thick substance composed of a monolayer hexagonal sp^2-hybridised carbon, has caught the interest of researchers in recent years due to its unique structure and exceptional electrical, mechanical, thermal, and optical properties [1-6]. These properties can be enhanced further by fusing graphene sheets with nanoscale or micron-sized transition metal oxides to produce unique graphene-based composites. To achieve exceptional hybrid characteristics in graphene-based composites, a variety of transition metal oxide structures have been linked to graphene layers [7-18]. Zinc oxide (ZnO), a wide-bandgap (3.37 eV) semiconductor, is a transition metal oxide that has drawn considerable research attention due of its distinctive properties. With a significant exciton binding energy of 60 MeV at ambient temperature, ZnO is a non-toxic, environmentally friendly, and readily available material with a cheap production cost. The multifunctional nature of ZnO, which is modifiable by changing its morphology and crystallinity, has attracted a lot of attention in the last two decades [19]. ZnO hollow microspheres are of interest in many technological applications such as solar cells [20-22], lithium-ion batteries [23,24], photocatalysis [25-27], sensors [28-30], supercapacitor electrode materials [31,32] and medical [33] because of their low density, high surface area and hollow geometrical shapes.

Hybridisation of different materials allows the generation of composites with versatile and tailor-made properties, demonstrating attractive combinations that outperform the individual components [34]. Considering the outstanding properties of graphene and ZnO, the generation of graphene-ZnO

composite is expected to provide exceptional performance. However, the solvothermal synthesis of graphene-ZnO hollow microspheres composite has received little attention.

A graphene-zinc oxide hollow microspheres (rGS-ZnO(HMs)) composite was synthesised utilising a solvothermal processing approach in this study. This one-pot synthesis process is straightforward, efficient, and requires no reducing or oxidising chemicals. In situ growth of ZnO on the surface of graphene produced uniformly adorned hollow microspheres. The morphology and electrochemical properties of the rGS-ZnO(HMs) composite was thoroughly examined.

Experimental

Materials. Cheap Tubes Inc. (Grafton, US) provided commercially available graphene oxide (GO, 99 wt%) powder. Zinc acetate dihydrate (Zn(CH3COO)2.2H2O, 99.5%) and absolute ethanol were supplied by Merck and HmbG Chemicals, respectively. No further purification was performed on any of the chemicals, and distilled water was used throughout the sample preparation process.

Solvothermal preparation of rGS-ZnO(HMs) composite. GO powder was dissolved in absolute ethanol to achieve a concentration of 1 mg/ml of GO and stirred continuously for 30 minutes. Subsequently, 2.5 mM of $Zn(CH_3COO)_2.2H_2O$ was added and the mixture suspension was sonicated for 30 minutes to obtain a homogeneous solution. The suspension was then transferred into a Teflon-lined autoclave. The autoclave was sealed and maintained in the oven at 180 °C for 24 hours. After cooling the autoclave to room temperature naturally, the black precipitates were separated by centrifugation, and washed with distilled water and absolute ethanol repeatedly. The pure rGS-ZnO(HMs) composite powder was dried in the oven at 60 °C for 8 hours. For comparison purposes, a control experiment was performed without adding zinc precursor and the product was labelled as rGS.

Morphological characterization of rGS-ZnO(HMs) composite. The X-ray diffraction (XRD) spectra on powdered samples was collected via a Bruker.D8 Advance 9 Position diffractometer using Cu K-α radiation ($\lambda = 0.15406$ nm) to determine the crystalline phase of the samples. The disordering of the formed carbon was examined using Raman spectroscopy (Renishaw inVia system with a laser of 25 mV at 532 nm). A field emission scanning electron microscope (FESEM, Zeiss Merlin) and a transmission electron microscope (TEM, Philips CM12) were used to analyse the structural morphology of G-ZnO(HMs) composites.

Preparation of electrodes and electrochemical characterization. To evaluate the electrochemical characteristics of the composite, electrodes were prepared by mixing the electroactive materials, carbon black, and poly(vinylidenefluoride-hexafluoropropylene) (PVDF-HFP) binder in a mass ratio of 90: 5: 5. A small amount of acetone was added to the mixture to produce a homogeneous slurry paste, which was coated on graphite tape and dried overnight in an oven at 60 °C overnight. An electrochemical cell was assembled by sandwiching two symmetric electrodes separated by a 25 μm thickness of microporous membrane (Celgard 3501, LLC) as a separator in a 6M KOH electrolyte.

The performance of the electrochemical cells was studied using cyclic voltammetry (CV), galvanostatic charge-discharge (GCD) and electrochemical impedance (EIS) on a Solartron SI 1286 Electrochemical Interface and a Solartron HF 1255 Frequency Response Analyzer. All the measurements were carried out at room temperature (25 °C). The CV measurement was conducted within a potential range of 0 to 1 V and over a range of scan rates from 1 to 100 mV/s. The GCD measurement was conducted over a potential range of 0 to 1 V and at a current density of 0.1 to 1.0 A/g. EIS data were recorded at 10 mV over a frequency range of 1 MHz to 10 mHz.

Results and discussion

Morphological characteristics. The XRD patterns of the GO, rGS and rGS-ZnO(HMs) composite are shown in Fig. 1(a). The presence of oxygenated functional groups attached to the basal planes and edges of carbon sheets is associated with the peak emerging at around 11.0° in the GO pattern [36]. Meanwhile, the development of small bumps at 23.5° and 42.8° in the rGS pattern confirms the

reduction of GO to rGS, or reduced graphene oxide [35,36]. These bumps imply the loss of a substantial number of oxygen-containing groups and the formation of much more disordered graphene sheets. The rGS-ZnO(HMs) composite diffraction peaks at 31.9°, 34.5°, 36.3°, 47.6°, 56.7°, 62.9°, 66.4°, 67.9°, 69.3°, 72.5° and 77.0° correspond well with the hexagonal phase wurtzite of the ZnO structure, which is consistent with the reference pattern JPCDS 36-1451 [37]. There were no peaks of any contaminants observed, implying that high-quality ZnO nanoparticles were synthesised. The diffraction peaks are extremely sharp and intense, indicating the formation of a well-crystalline structure of ZnO nanoparticles on the graphene surface. The absence of the GO peak implies that GO was completely reduced throughout the hybridisation process. There are no rGS diffraction peaks in the rGS-ZnO(HMs) composite due to the extensive formation of ZnO and the comparatively low amount of rGS [36,38].

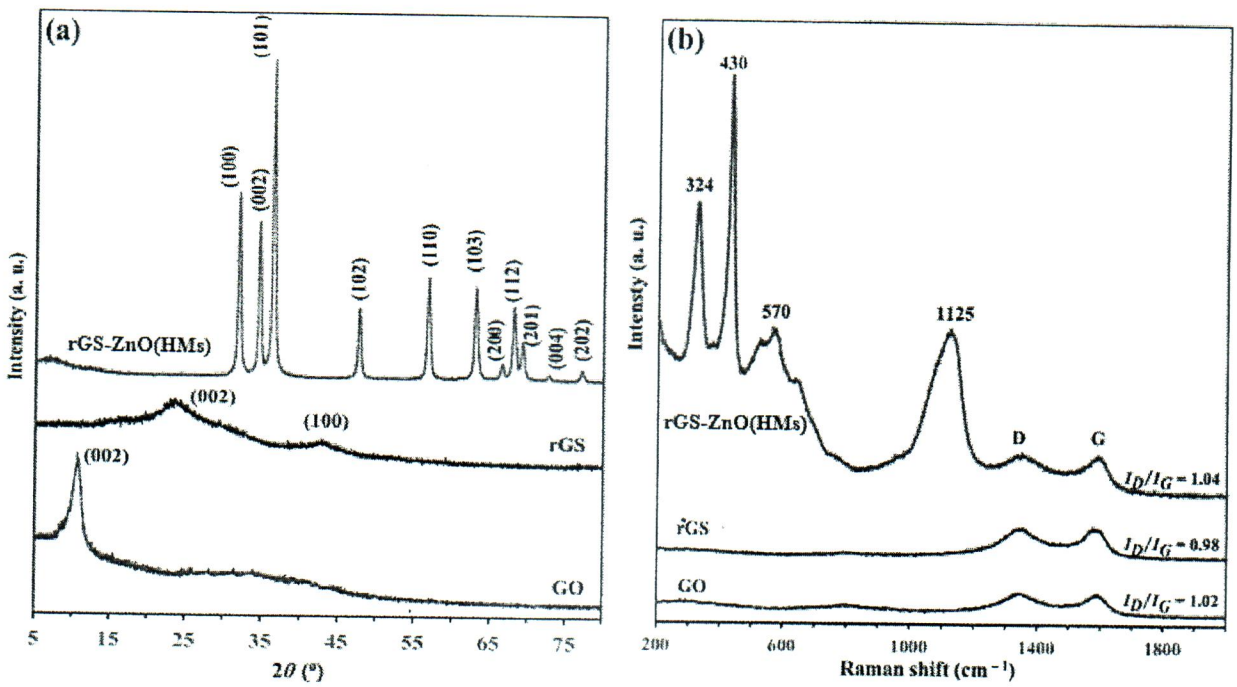

Fig. 1. (a) XRD spectra, and (b) Raman spectra for GO, rGS and rGS-ZnO(HMs) composite

The presence of both carbon and ZnO in the structure of the prepared rGS-ZnO(HMs) composite can be confirmed from the Raman spectra. As shown in Fig. 1(b), the characteristic Raman peaks of the rGS-ZnO(HMs) composite exhibit D and G bands at around 1347 cm^{-1} and 1589 cm^{-1}, respectively. The G band provides useful information on in-plane stretching vibrations of symmetric sp^2 C-C bonds, while the D band is associated with the disturbance of the hexagonal graphitic lattice [39, 40]. Compared with rGS, the D and G bands in the rGS-ZnO(HMs) composite were blue-shifted by 5 cm^{-1} and 14 cm^{-1}, respectively. These shifts are assigned to the chemical interaction between ZnO and rGS, which suggests that the electronic structure of the rGS could be modified by contacting it with ZnO nanoparticles [35]. The intensity ratio of the D band to the G band, I_D/I_G can be used to measure the relative defect content in the sp^2 carbon lattice [41]. The calculated I_D/I_G ratios for GO, rGS and the rGS-ZnO(HMs) composite are 1.02, 0.98, and 1.04, respectively. The I_D/I_G ratio of rGS is smaller than that of GO, which suggests an increase in the average size of the in-plane sp^2 domains upon reduction of GO. The relatively high I_D/I_G ratio for GO is contributed by the presence of oxygenated functional groups on both sides and edges of the GO sheets [42]. However, the rGS-ZnO(HMs) composite exhibits the highest I_D/I_G ratio due to the increasing disorder of sp^2 domains contributed by the presence of ZnO nanoparticles on the graphene sheets. The rGS-ZnO(HMs) composite curve displayed four distinctive Raman vibration modes centred at 324 cm^{-1}, 430 cm^{-1}, 570 cm^{-1} and 1125 cm^{-1}, which are referred to as the ZnO spectrum. The edge at about 324 cm^{-1} has been assigned to the second order Raman scattering (E_2 (high)-E_2 (low) mode) and arises from the zone-

boundary phonon of hexagonal ZnO [43]. The intense peak at 430 cm^{-1} corresponds to the nonpolar optical phonon E_2 (high) mode, which is known as the Raman active optical phonon mode and is related to the motion of oxygen atoms [40,44]. The presence of the E_2 (high) mode in the composite samples, which is characteristic of wurtzite hexagonal phase ZnO is consistent with the above XRD analysis. The peak at 570 cm^{-1} is assigned to the E_1 longitudinal optical (E_1 (LO)) mode, attributed to oxygen deficiency defects in ZnO [43]. The broad band at 1125 cm^{-1} is due to the multiple-phonon scattering processes ($2A_1$ (LO), $2E_1$ (LO) and 2LO mode), characteristic of the II-IV semiconductor [40,45].

FESEM was used to examine the surface morphology of the as-prepared rGS-ZnO(HMs) composite. Homogeneous ZnO hollow microspheres were discovered to anchor the graphene structure (Fig. 2(a)). The microspheres had diameters ranging from 800 to 1200 nm and were equally distributed on the graphene surface. As demonstrated in the high-magnification image (Fig. 2(b)), the microspheres are made up of ZnO nanoparticles about 30 nm in diameter, which is consistent with the XRD findings. TEM examination was also used to analyse the structure of the ZnO hollow microspheres formed on the surface of graphene. The fact that the middle portion of the microsphere is lighter than the edge clearly confirms the hollow interiors of the unique ZnO microspheres (Fig. 2(c)).

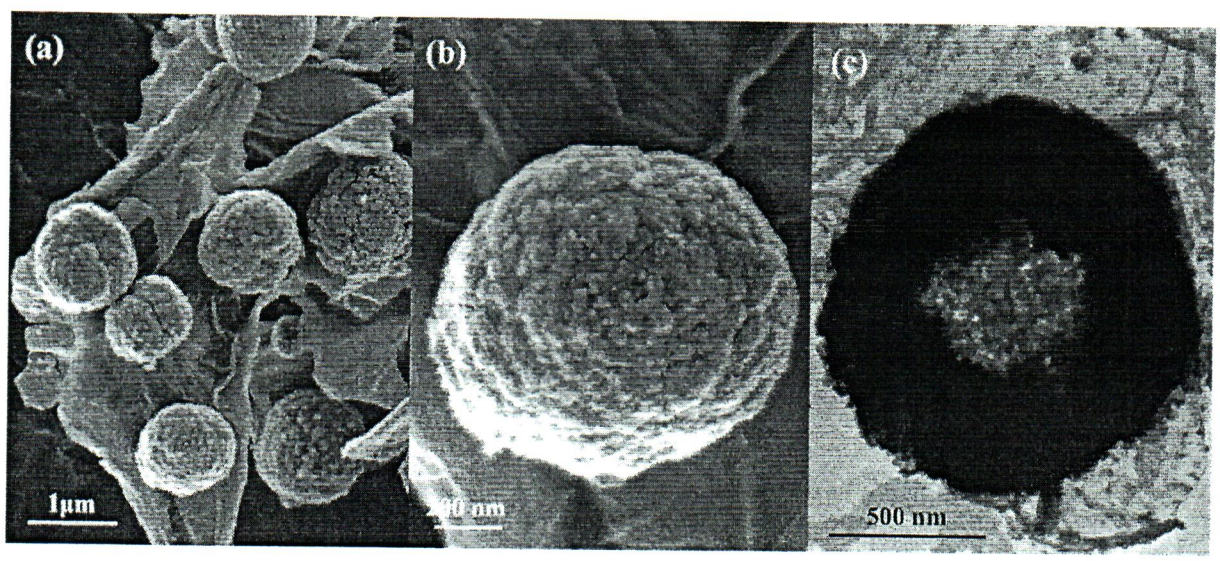

Fig. 2. FESEM images of (a) rGS-ZnO(HMs) composite and (b) rGS-ZnO(HMs) composite with high-magnification; (c) TEM images of a single ZnO hollow sphere

Formation mechanism of rGS-ZnO(HMs) composite. The formation mechanism of ZnO hollow microspheres on graphene sheets is shown in Fig. 3. GO contains large amounts of epoxide, hydroxyl and carboxyl acid reactive groups on its surface and edges. These functional groups immobilise Zn^{2+} ions through C–O–Zn bonds, thereby undergoing condensation reactions, enabling Zn^{2+} to be connected to these nucleation sites and ZnO quantum dots grown on graphene sheets *via* normal ionic bonds [46]. The high temperature inside the autoclave stimulates the nucleation and subsequent growth of ZnO quantum dots to form nanoparticles. Simultaneously, due to the high temperature condition, ethanol can effectively remove most of the oxygen-functional groups and restore the conjugated network of the graphitic lattice of GO, resulting in the rGS [47]. The ZnO nanoparticles preferentially aggregate and self-assemble into metastable spheres by the well-known growth mechanism of "oriented attachment" to minimise the total surface energy [48]. In a prolonged solvothermal process, the inner phase of metastable ZnO microspheres with higher energy will move to the stable outer surface through Ostwald ripening, resulting in the hollow structure.

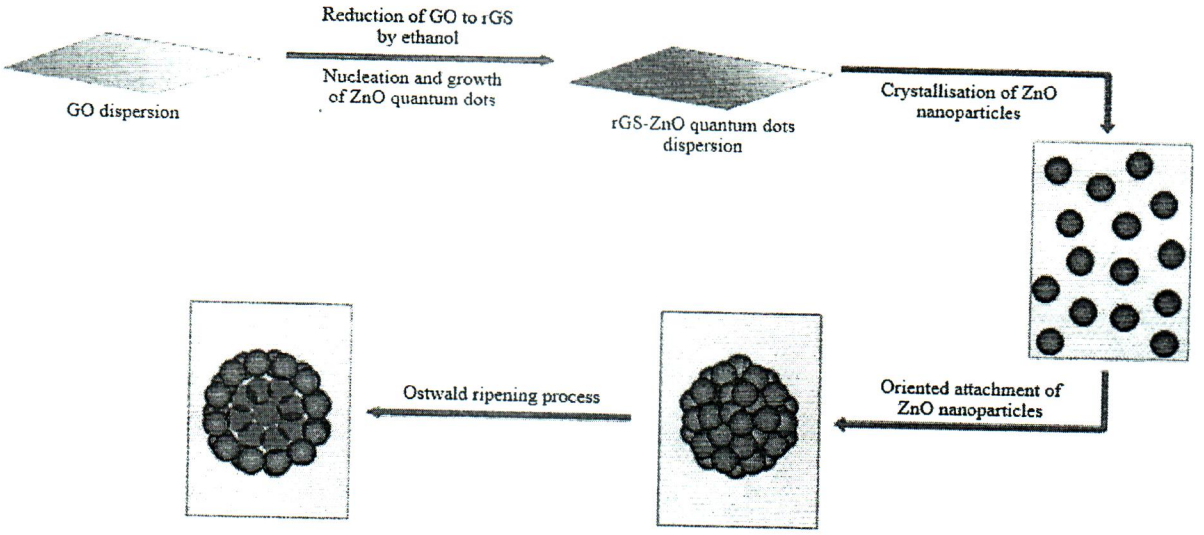

Fig. 3. Schematic of the formation mechanism of ZnO hollow microsphere on rGS sheet

Electrochemical Characteristics. Cyclic voltammetry (CV) is a well-known electrochemical technique for studying a material's capacitive properties. At a scan rate of 1 mV/s, Fig. 4(a) compares the CV profiles of rGS and rGS-ZnO(HMs). The CV curves have an irregular quasi-rectangular form with no distinct pair of redox peaks during the anodic and cathodic sweeps, indicating that capacitance is driven by a combination of EDLCs and faradaic redox activities. At the same scan rate, the rGS-ZnO(HMs) composite electrode had a larger integrated area than the rGS electrode, confirming improved charge storage ability. This clearly shows that deposition of ZnO hollow microspheres on the surface of rGS enhances the electrode's total capacitance. The specific capacitance, C_{sp} of the samples can be determined from the CV curves using Eq. (1) [42].

$$C_{sp} = \frac{\int i}{m * s} \tag{1}$$

where $\int i$ is the integrated area of the CV curve, m is the mass of the electrode material in grams, and s is the scan rate in volts per second. At a scan rate of 1 mV/s, the calculated C_{sp} values for these electrochemical capacitors were 40.7 F/g (rGS-ZnO(HMs)) > 10.9 F/g (rGS). The CV curves for the rGS-ZnO(HMs) electrode at various scan rates were examined to learn more about its capacitive behaviour (Fig. 4(b)). It was discovered that as the scan rate increased from 1 to 100 mV/s, the integral area of the curves decreased. The result clearly indicates that specific capacitance reduces steadily as scan rates increase. At scan rates of 1, 10, 30, 50, 70, and 100 mV/s, the specific capacitance of the rGS-ZnO(HMs) electrode was calculated to be 40.7, 32.3, 16.3, 11.0, 8.8, and 7.4 F/g, respectively (Fig. 4(c)). The specific capacitance rapidly declines with rising scan rates, which can be attributed to insufficient time available for ion diffusion and adsorption within the intrinsic pore structures of the active material at high scan rates. This diffusion effect restricts electrolytic ion movement, rendering some active surface areas inaccessible for charge storage [34,49].

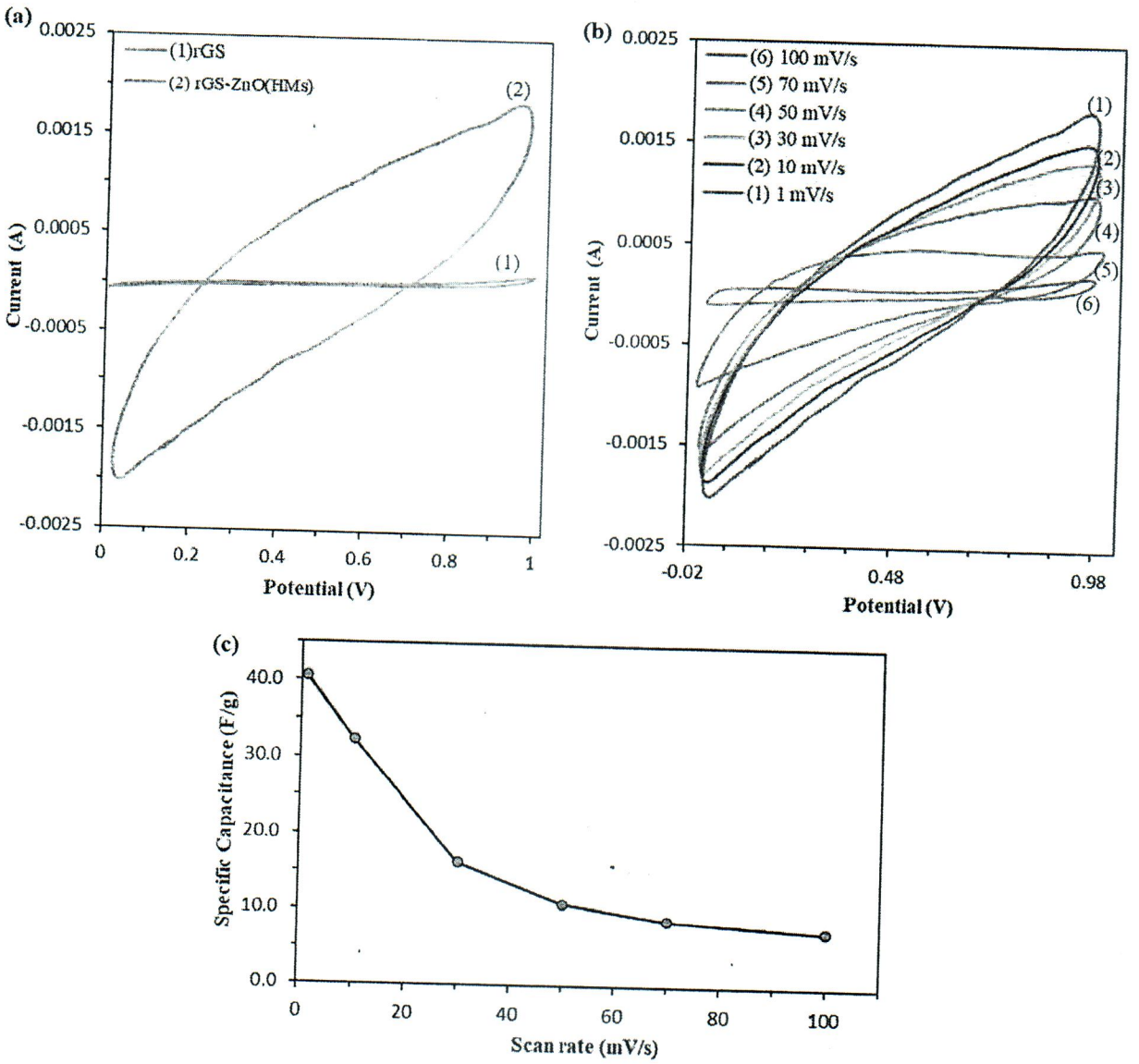

Fig. 4. Cyclic voltammograms (CV) curves of (a) rGS and rGS-ZnO(HMs) at a scan rate of 1 mV/s, (b) rGS-ZnO(HMs) at different scan rates, and (c) variation of specific capacitance of rGS-ZnO(HMs) at different scan rates

A galvanostatic charge-discharge test was used to further investigate the electrochemical performance of the electrodes by applying a series of charging and discharging currents to the electrochemical capacitors. The voltage response of rGS and rGS-ZnO(HMs) composite electrodes at a constant current density of 1.00 A/g is shown in Fig. 5(a). The galvanostatic charge-discharge diagram is nearly symmetrical triangular, with a little bend in the charging curve for the rGS electrode, indicating electric double layer capacitive behaviour. The asymmetric design of the device could explain the bend in the charging curve. Meanwhile, the rGS-ZnO(HMs) composite curve deviates significantly from the triangular form, indicating the involvement of the ZnO Faradaic reaction process. This composite curve depicts three types of potential variation in the discharge range. A sudden drop in current at the start of discharge is caused by the electrode's internal resistance (region I), a linear variation in the time dependence of the potential indicates double-layer capacitance behaviour (region II), which is caused by charge separation at the electrode-electrolyte interface, and a slope variation in the time dependence of the potential (region III) indicates typical pseudo-capacitance behaviour, which results from the electrochemical adsorption/desorption or a redox reaction at an electrode-electrolyte interface [50]. When comparing their individual masses, the rGS-ZnO(HMs) composite

electrode has lower internal resistance and thus a larger specific capacitance than the rGS electrode. The specific capacitance of the rGS-ZnO(HMs) composite is quite similar to the CV analysis result.

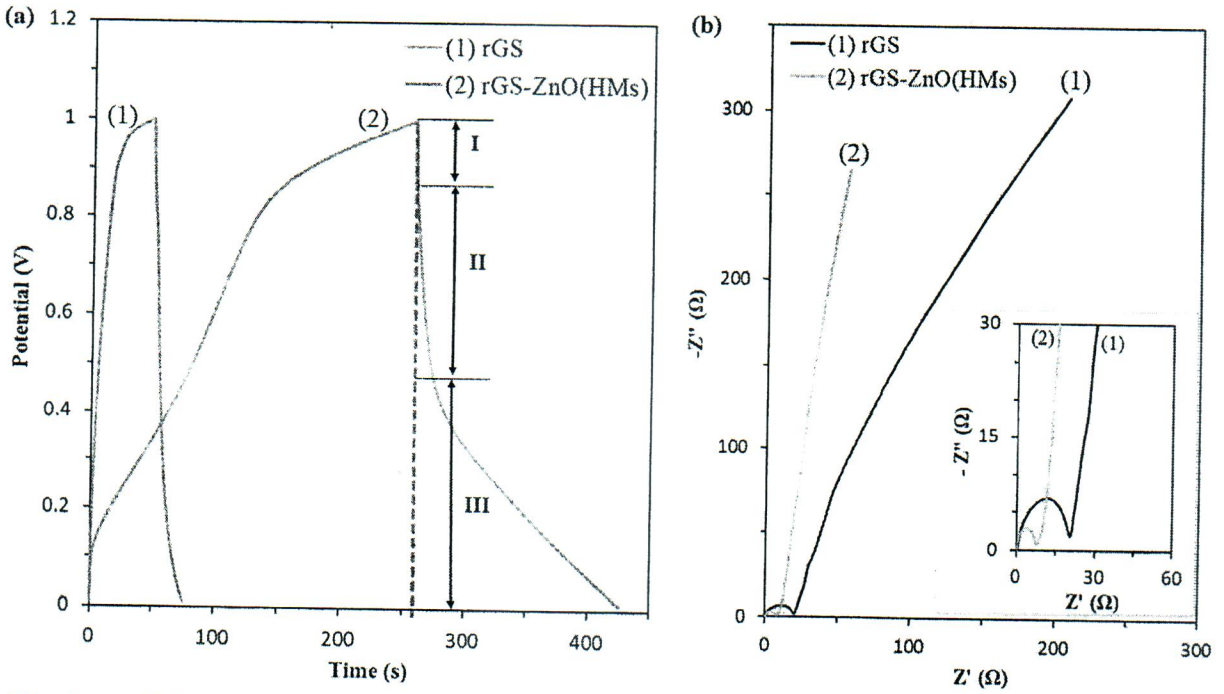

Fig. 5. (a) Galvanostatic charge-discharge curves at a current density of 1.00 A/g and (b) Nyquist plots at 10 mV of rGS and rGS-ZnO(HMs) composite electrodes

Accordingly, the specific energy, E_{sp} and specific power, P_{sp} were calculated from the GCD data using the equations:

$$E_{sp} = \frac{CV^2}{2m} \tag{2}$$

$$P_{sp} = \frac{E_{sp}}{t} \tag{3}$$

where C is specific capacitance estimated from charge-discharge curves, V is the potential range during discharge, t is the discharge time and m is the total mass of electroactive material of the electrodes. Their maximum values are tabulated in Table 1.

Analysing the resistive behaviour of electrode materials using electrochemical impedance spectroscopy (EIS) is a helpful approach. The Nyquist plots of rGS and rGS-ZnO(HMs) composite electrodes at 10 mV are shown in Fig. 5(b). The semicircles visible in the high frequency region correspond to the electronic resistance within the electrode materials, which is induced by the charge transfer process at the electrode/electrolyte interface. Meanwhile, the ion diffusion in the electrolyte is represented by the steeply rising straight line in the low frequency region. The equivalent series resistance (ESR) is defined as the initial x-intercept point of the semicircle, which combines the bulk resistance of the electrode electroactive material, the bulk resistance of the electrolyte, and the interface resistance between the electrode material and the current collector [51]. The faradaic charge transfer resistance, R_{ct} is equal to the diameter of the semicircle arc on the real axis [52]. The smaller diameter semicircle promotes rapid electron transport between electrode material and electrolyte. Table 1 shows the ESR and R_{ct} values calculated from the Nyquist plot in Fig. 5(b) for the rGS and rGS-ZnO(HMs) composite electrodes. The higher ESR and R_{ct} values of the rGS electrode strongly suggest that attaching ZnO hollow microspheres to the surface of graphene sheets increases charge transfer.

Table 1
Electrochemical parameters of rGS and rGS-ZnO(HMs) composite electrodes.

Sample	ESR (Ω)	R_{ct} (Ω)	Specific capacitance (F/g)	Energy density (Wh/kg)	Power density (kW/kg)
rGS	0.49	20.01	10.9	0.81	0.63
rGS-ZnO(HMs)	0.38	7.55	40.7	5.75	1.79

Conclusions

A one-step solvothermal process was used to synthesise the rGS-ZnO(HMs) composite as an electrode material for supercapacitors. The surface morphology, microstructure, composition, and electrochemical behaviour of the composite material have all been comprehensively investigated. FESEM and TEM images revealed a homogeneous distribution of ZnO hollow microspheres on the rGS sheet substrate. The microspheres are constructed of ZnO nanoparticles about 30 nm in diameter. The electrochemical performance of the rGS-ZnO(HMs) composite electrode is greatly improved over that of the rGS electrode. The increased supercapacitance performance of the rGS-ZnO(HMs) composite was attributable mostly to the intrinsic double-layer capacitance of the rGS sheets and the pseudocapacitance of the ZnO microspheres.

Acknowledgements

Financial support has been gratefully acknowledged from the Universiti Pertahanan Nasional Malaysia (UPNM) Geran Penyelidikan Jangka Pendek (UPNM/2020/GPJP/SG/6) and the Malaysian Ministry of Higher Education (MOHE). The authors are also grateful to the Centre for Research and Instrumentation (CRIM) at Universiti Kebangsaan Malaysia (UKM) for providing access to its analytical equipment.

References

[1] S.K. Abdel-Aal, A.S. Abdel-Rahman, Graphene influence on the structure, magnetic, and optical properties of rare-earth perovskite, J Nanopart Res 22 (2020) 267: 1-10.

[2] G. Jing, Z. Ye, J. Wu, S. Wang, X. Cheng, V. Strokova, V. Nelyubova, Introducing reduced graphene oxide to enhance the thermal properties of cement composites, Cem Concr Compos 109 (2020) 103559: 1-10.

[3] N. Khobragade, K. Sikdar, B. Kumar, S. Bera, D. Roy, Mechanical and electrical properties of copper-graphene nanocomposite fabricated by high pressure torsion, J. Alloys Compd 776 (2019) 123-132.

[4] R. Aradhana, S. Mohanty, S.K. Nayak, Comparison of mechanical, electrical, and thermal properties in graphene oxide and reduced graphene oxide filled epoxy nanocomposite adhesives, Polymer 141 (2018) 109-123.

[5] K. Chu, X.-h. Wang, Y.-b. Li, D.-j. Huang, Z.-r. Geng, X.-l. Zhao, H. Liu, H. Zhang, Thermal properties of graphene/metal composites with aligned graphene, Mater. Des 140 (2018) 85-94.

[6] S. Prabhu, M. Pudukudy, S. Sohila, S. Harish, M. Navaneethan, D. Navaneethan, R. Ramesh, Y. Hayakawa, Synthesis, structural and optical properties of ZnO spindle/reduced graphene oxide composites with enhanced photocatalytic activity under visible light irradiation, Opt. Mater. 79 (2018) 186-195.

[7] Z. Wang, Z. Jia, Q. Li, X. Zhang, W. Sun, J. Sun, B. Liu, B. Ha, The enhanced NO_2 sensing properties of SnO_2 nanoparticles/reduced graphene oxide composite, J. Colloid Interface Sci. 537 (2019) 228-237.

[8] S. Zuo, D. Li, Z. Wu, Y. Sun, Q. Lu, F. Wang, R. Zhuo, D. Yan, J. Wang, P. Yan, SnO_2/graphene oxide composite material with high-rate performance applied in lithium storage capacity, Electrochim. Acta 264 (2018) 61-68.

[9] H.E. Marouazi, P. Jiménez-Calvo, E. Breniaux, C. Colbeau-Justin, I. Janowska, V. Keller, Few Layer Graphene/TiO_2 Composites for Enhanced Solar-Driven H_2 Production from Methanol, ACS Sustain. Chem. Eng. 9 (2021) 3633-3646.

[10] M. Ruidíaz-Martínez, M.A. Álvarez, M.V.López-Ramón, G. Cruz-Quesada, J. Rivera-Utrilla, M. Sánchez-Polo, Hydrothermal Synthesis of rGO-TiO_2 Composites as High-Performance UV Photocatalysts for Ethylparaben Degradation, Catalyst 10 (2020) 520: 1-25.

[11] J. Azuaje, A. Rama, A. Mallo-Abreu, M.G. Boado, M. Majellaro, C.R. Tubío, R. Prieto, X. García-Mera, F. Guitian, E. Sotelo, Alvaro Gil, Catalytic performance of a metal-free graphene oxide-Al_2O_3 composite assembled by 3D printing, J. Eur. Ceram. Soc. 41 (2021) 1399-1406.

[12] J. Li, J. Ji, J. Chen, W. Zhang, Synthesis of TiO_2/reduced graphene oxide–$Al2O_3$ composites and their advanced properties for photocatalysis, J. Nanoparticle Res. 22 (2020) 224: 1-12.

[13] X. Hu, Y. Yu, S. Ren, N. Lin, Y. Wang, J. Zhou, Highly efficient removal of phenol from aqueous solutions using graphene oxide/Al_2O_3 composite membrane, J. Porous Mater. 25 (2018) 719-726.

[14] K.-Y. Chen, S. Gupta, N.-H. Tai, Reduced graphene oxide/Fe_2O_3 hollow microspheres coated sponges for flexible electromagnetic interference shielding composites, Compos. Commun. 23 (2021) 100572: 1-7.

[15] F. Wang, X. Li, Z. Chen, W. Yu, K.P. Loh, B. Zhong, Y. Shi, Q.-H. Xu, Efficient low-frequency microwave absorption and solar evaporation properties of γ-Fe_2O_3 nanocubes/graphene composites, Chem. Eng. J. 405 (2021) 126676: 1-10.

[16] Z. Zhou, C. Ding, W. Peng, Y. Li, F. Zhang, X. Fan, One-step fabrication of two-dimensional hierarchical Mn_2O_3@graphene composite as high-performance anode materials for lithium-ion batteries, J. Mater. Sci. Technol. 80 (2021) 13-19.

[17] H. Han, Q.A. Sial, S.S. Kalanur, H. Seo, Binder assisted self-assembly of graphene oxide/Mn_2O_3 nanocomposite electrode on Ni foam for efficient supercapacitor application, Ceram. Int. 46 (2020) 15631-15637.

[18] D.R. Rout, S. Chaurasia, H.M. Jena, Enhanced photocatalytic degradation of malachite green using manganese oxide doped graphene oxide/zinc oxide (GO-ZnO/Mn_2O_3) ternary composite under sunlight irradiation, J. Environ. Manage. 318 (2022) 115449: 1-14.

[19] M.K. Kavitha, H. John, P. Gopinath, R. Philip, Synthesis of reduced graphene oxide-ZnO hybrid with enhanced optical limiting properties, J. Mater. Chem. C 1 (2013) 3669-3676.

[20] L. Yu, W. Hao, Z. Li, X. Ren, H. Yang, H. Ma, Synthesis of ZnO core/shell hollow microspheres to boost light harvesting capability in quantum dots-sensitized solar cell, Chem. Phys. Lett. 764 (2021) 138283: 1-6.

[21] A. Banik, M.S. Ansari, M. Qureshi, Efficient Energy Harvesting in SnO_2-Based Dye Sensitized Solar Cells Utilizing Nano-Amassed Mesoporous Zinc Oxide Hollow Microspheres as Synergy Boosters, ACS Omega 3 (2018) 14482-14493.

[22] L. Wang, C. Ma, X. Ru, Z. Guo, D. Wu, S. Zhang, G. Yu, Y. Hu, J. Wang, Facile synthesis of ZnO hollow microspheres and their high performance in photocatalytic degradation and dye sensitized solar cells, J. Alloys Compd. 647 (2015) 57-62.

[23] G. Wua, Z. Jiaa, Y. Cheng, H. Zhang, X. Zhou, H. Wu, Easy synthesis of multi-shelled ZnO hollow spheres and their conversion into hedgehog-like ZnO hollow spheres with superior rate performance for lithium-ion batteries, Appl. Surf. Sci. 464 (2019) 472-478.

[24] S.-C. Weng, S. Brahma, C.-C. Chang, J.-L. Huang, Synthesis of self-assembled Hollow-Sphere ZnO/rGO Nanocomposite as Anode Materials for Lithium-Ion Batteries, Int. J. Electrochem. Sci. 14 (2019) 3727-3739.

[25] L. Zhou, Z. Han, G.-D. Li, Z. Zha, Template-free synthesis and photocatalytic activity of hierarchical hollow ZnO microspheres composed of radially aligned nanorods, J. Phys. Chem. Solids 148 (2021) 109719: 1-8.

[26] C. Chen, X. Liu, Q. Fang, X. Chen, T. Liu, M. Zhan, Self-assembly synthesis of CuO/ZnO hollow microspheres and their photocatalytic performance under natural sunlight, Vacuum 174 (2020) 109198: 1-7.

[27] M.R. Hernández, A.d.L. Santillán, E.d.C. Ortiz, S.F. Tavizón, I. Moggio, E. Arias, C.A. Gallardo-Vega, J.A.M. Silva, E.D. Barriga-Castro, Hollow ZnO microspheres functionalized with electrochemical graphene oxide for the photodegradation of salicylic acid, RSC Adv. 9 (2019) 6965-6972.

[28] H. Wang, Y. Yang, T. Xie, Y. Lin, Highly Sensitive and Selective HCHO Sensor Based on Co Doped ZnO Hollow Microspheres Activated by UV Light, IEEE Sens. J. 21(6) (2021) 7558-7564.

[29] S. Wang, G. Qiao, X. Chen, X. Wang, H. Cui, Synthesis of ZnO Hollow Microspheres and Analysis of Their Gas Sensing Properties for *n*-Butanol, Crystals 10 (2020) 1010: 1-11.

[30] M. Xiao, Y. Li, B. Zhang, G. Sun, Z. Zhang, Synthesis of g-C3N4-Decorated ZnO Porous Hollow Microspheres for Room-Temperature Detection of CH4 under UV-Light Illumination, Nanomaterials 9 (2019) 1507: 1-13.

[31] A.L. Albert, S. Radiman, M.A.A. Hamid, M.F.Y.M. Hanappi, Physical and Electrochemical Properties of Graphene Decorated with ZnO Hollow Spheres for Supercapacitor Applications, Key Engineering Materials 908 (2022) 284-292.

[32] G.-C. Li, P.-F. Liu, R. Liu, M. Liu, K. Tao, S.-R, Zhu, M.-K. Wu, F.-Y. Yia, L. Han, MOF-derived hierarchical double-shelled NiO/ZnO hollow spheres for high-performance supercapacitor, Dalton Trans. 45(34) (2016) 13311-13316.

[33] N. Puvvada, S. Rajput, B.N.P. Kumar, S. Sarkar, S. Konar, K.R. Brunt, R.R. Rao, A. Mazumdar, S.K. Das, R. Basu, P.B. Fisher M. Mandal, A. Pathak, Novel ZnO hollow-nanocarriers containing *paclitaxel* targeting folate-receptors in a malignant pH-microenvironment for effective monitoring and promoting breast tumour regression, Sci. Rep. 5 (2015) 11760.

[34] A. Ramadoss, S.J. Kim, Improved activity of a graphene-TiO_2 electrode in an electrochemical supercapacitor, Carbon 63 (2013) 434-445.

[35] F.S. Omar, H.N. Ming, S.M. Hafiz, L.H. Ngee, Microwave Synthesis of Zinc Oxide/Reduced Graphene Oxide Hybrid for Adsorption-Photocatalysis Application, Int. J. Photoenergy 2014 (2014) 1-8.

[36] T. Lv, L. Pan, X. Liu, T. Lu, G, Zhu, Z. Sun, Enhanced photocatalytic degradation of methylene blue by ZnO-reduced graphene oxide composite synthesized via microwave-assisted reaction, J. Alloys Compd. 509 (2011) 10086-10091.

[37] Y.-M. Lu, C.-F. Tseng, B.-Y. Lan, C.-F. Hsieh, Fabrication of Graphene/Zinc Oxide Nano-Heterostructure for Hydrogen Sensing, Materials 14 (2021) 6943.

[38] J. Qina, X. Zhang, C.Yang, M. Cao, M. Ma, R. Liu, ZnO microspheres-reduced graphene oxide nanocomposite for photocatalytic degradation of methylene blue dye, Appl. Surf. Sci. 392 (2017) 196-203.

[39] F.S. Ghoreishi, V. Ahmadi, M. Samadpour, Improved performance of CdS/CdSe quantum dots sensitized solar cell by incorporation of ZnO nanoparticles/reduced graphene oxide nanocomposite as photoelectrode, J. Power Sources 271 (2014) 195-202.

[40] S.S. Low, H.-S. Loh, J.S. Boey, P.S. Khiew, W.S. Chiu, M.T.T. Tan, Sensitivity enhancement of graphene/zinc oxide nanocomposite-based electrochemical impedance genosensor for single stranded RNA detection, Biosens. Bioelectron 94 (2017) 365-373.

[41] J. Rodrigues, J. Zanoni, G. Gaspar, A.J.S. Fernandes, A.F. Carvalho, N.F. Santos, T. Monteiro, F.M. Costa, ZnO decorated laser-induced graphene produced by direct laser scribing, Nanoscale Adv. 1 (2019) 3252-3268.

[42] S.P. Lim, N. M. Huang, H. N. Lim, Solvothermal synthesis of SnO_2/graphene nanocomposites for supercapacitor application, Ceram. Int. **39** (2013) 6647-6655.

[43] P. Kumar, V. Singh, V. Sharma, G. Rana, H.K. Malik, K. Asokan, Investigation of phase segregation in yttrium doped zinc oxide, Ceram. Int. 41 (2015) 6734-6739.

[44] D.H. Xu, W.Z. Shen, Cu-Doped ZnO Hemispherical Shell Structures: Synthesis & Room-Temperature Ferromagnetism Properties, J. Phys. Chem. C 116(24) (2012) 13368-13373.

[45] D.A. Guzmán-Embús, M.O. Cardozo, C. Vargas-Hernández, Genomic DNA characterization of pork spleen by Raman spectroscopy, J. Appl. Phys. 114 (2013) 194704: 1-8.

[46] A. Tayyebi, M. outokesh, M. Tayebi, A. Shafikhâni, S.S. Şengör, ZnO quantum dots-graphene composites: Formation mechanism and enhanced photocatalytic activity for degradation of methyl orange dye, J. Alloys Compd. 663 (2016) 738-749.

[47] Z.-g. Wang, P.-j. Li, Y.-f. Chen, J.-r. He, B.-j. Zheng, J.-b. Liu, F. Qi, The green synthesis of reduced graphene oxide by the ethanol-thermal reaction and its electrical properties, Mater. Lett. 116 (2014) 416-419.

[48] C.-X. He, B.-X. Lei, Y.-F. Wang, C.-Y. Su, Y.-P. Fang, D.-B. Kuang, Sonochemical preparation of Hierarchical ZnO Hollow spheres for efficient dye-sensitized cells, Chem. Eur. J. 16 (2010) 8757-8761.

[49] H.B. Li, M.H. Yu, F.X. Wang, P. Liu, Y. Liang, J. Xiao, C.X. Wang, Y.X. Tong, G.W. Yang, Amorphous nickel hydroxide nanospheres with ultrahigh capacitance and energy density as electrochemical pseudocapacitor materials, Nat. Commun. 4 (2013) 1894: 1-7.

[50] G.S. Gund, D.P. Dubal, B.H. Patil, S.S. Shinde, C.D. Lokhande, Enhanced activity of chemically synthesized hybrid graphene oxide/Mn_3O_4 composite for high performance supercapacitors, Electrochim. Acta 92 (2013) 205-215.

[51] M.F.Y.M. Hanappi, M. Deraman, M. Suleman, N.S.M. Nor, N.E.S. Sazali, E. Hamdan, N.S.M. Tajuddin, N.H. Basri, M.R.M. Jasni, M.A.R.Othman, Influence of aqueous KOH and H_2SO_4 electrolytes ionic parameters on the performance of carbon-based supercapacitor electrodes, Functional Materials Letters 3 (2017) 1750013: 1-5.

[52] S. Ghasemi, R. Hosseinzadeh, M. Jafari, MnO2 nanoparticles decorated on electrophoretically deposited graphene nanosheets for high performance supercapacitor, Int. J. Hydrog. Energy 40 (2015) 1037-1046.